CHEMISTRY OF MATERIALS

ARTICLE

pubs.acs.org/cm

Low-Temperature Fluorination of Soft-Templated Mesoporous Carbons for a High-Power Lithium/Carbon Fluoride Battery

Pasquale F. Fulvio,[†] Suree S. Brown,[§] Jamie Adcock,[§] Richard T. Mayes,[†] Bingkun Guo,[†] Xiao-Guang Sun,[*,†] Shannon M. Mahurin,[†] Gabriel M. Veith,[*,‡] and Sheng Dai[*,†,§]

[†]Chemical Sciences Division and [‡]Materials Science and Technology Division, Oak Ridge National Laboratory, Oak Ridge, Tennessee 37831, United States

[§]Department of Chemistry, University of Tennessee, Knoxville, Tennessee 37996, United States

Supporting Information

ABSTRACT: Soft-templated mesoporous carbons and activated mesoporous carbons were fluorinated using elemental fluorine between room temperature and 235 °C. The mesoporous carbons were prepared via self-assembly synthesis of phloroglucinol−formaldehyde as a carbon precursor in the presence of triblock ethylene oxide−propylene oxide−ethylene oxide copolymer BASF Pluronic F127 as the template. The F/C ratios ranged from ∼0.15 to 0.75 according to gravimetric, energy dispersive X-ray spectroscopy, and X-ray photoelectron spectroscopy analysis. Materials have mesopore diameters up to 11 nm and specific surface areas as high as 850 $m^2 g^{-1}$ after fluorination as calculated from nitrogen adsorption isotherms at −196 °C. Furthermore, the materials exhibit higher discharge potentials and energy and power densities as well as faster reaction kinetics under high current densities than commercial carbon fluorides with similar fluorine contents when tested as cathodes for Li/CF_x batteries.

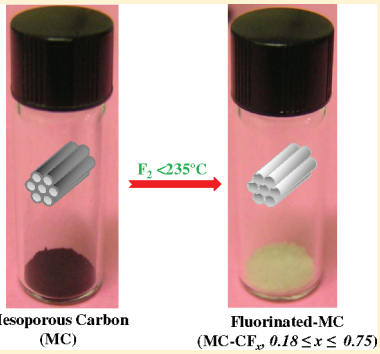

KEYWORDS: mesoporous carbon, low-temperature fluorination, Li/CF_x battery cathode, discharge potential, energy and power density

INTRODUCTION

CF_x batteries have the highest energy density among all primary lithium batteries with a theoretical value of 2180 W h kg^{-1}.[1,1−3] Currently available Li/CF_x batteries are limited to low rate applications due to their poor electronic conductivity and the layered nonporous structure of the cathode precursor material, namely, graphite.[4] In addition to natural graphite,[5,6] other nonporous and low surface area materials such as highly oriented pyrolitic graphite (HOPG),[7] carbon nanofibers (CNFs),[8,9] carbon nanotubes (CNTs),[10,11] fullerenes (C_{60}),[12−16] charcoal,[17] and carbons from petroleum cokes[2,18,19] have been fluorinated using different methods. Fluorination of carbon materials generates surface defects, such as $-CF_2/-CF_3$ groups which accommodate Li ions. Consequently, the specific capacity of the cells increases with the fluorine content.[2,9,18,19]

For all aforementioned materials, extreme temperatures and catalysts are required to obtain high F/C ratios and the final products are essentially nonporous and exhibit low surface areas (smaller than 100 $m^2 g^{-1}$). For instance, partially exfoliated graphitized carbon fibers with F/C ratios of 0.86 were obtained only after treatment at 480 °C.[8,9] Interestingly, graphitized carbons are generally unreactive in the presence of F_2, but were reactive toward fluorinating compounds such as NF_3 and ClF_3.[19] Elemental fluorine was found to react with graphitic carbons only in the presence of high oxidation state transition-metal fluorides, i.e., AgF_3, NiF_3, K_2NiF_6, and $KAgF_4$, after several days with a maximum F/C ratio of 0.83.[20,21]

In general, high temperatures and extents of fluorination induce the collapse of pore structures, which is detrimental for high rate capabilities in cathode materials. For example, CNTs with F/C ratios near 1 were only obtained after fluorinations at 600 °C, at which the tubular structure was destroyed and an amorphous carbon fluoride was obtained.[11] Petroleum coke-based carbons have more structural defects than natural graphite and CNTs and therefore are more easily fluorinated.[19] One way to prevent the loss of pores is to migrate from traditionally used graphite-based materials toward porous carbon substrates with a large number of defect sites (turbostratic carbon) and with enhanced accessibility to the CF sites provided by micro/mesopores. A recent example was demonstrated for ordered mesoporous carbons (OMCs), namely, CMK-1, prepared as inverse replicas of ordered mesoporous silica (OMS) MCM-48.[22,23] These OMCs were fluorinated by elemental fluorine at temperatures ranging from room temperature to 250 °C, much lower than those for graphite (>400 °C).[24] Such mesoporous carbons have an open hierarchical structure of accessible micro- and mesopores and turbostratic carbon walls. Both features allowed for the fluorination of the carbon frameworks at milder conditions. For instance, CMK-1 carbon fluorides with F/C ratios ranging from 0.1 to 0.5 were obtained after room

Received: April 30, 2011
Revised: August 26, 2011
Published: September 29, 2011

temperature and 150 °C reactions, respectively.[24] For higher F/C ratios of 0.8 prepared at 250 °C, however, the mesopore structure was lost during fluorination.[24] The instability of CMK-1 toward direct fluorination is intrinsic to its nanostructure, which is composed of mesopores formed by voids between interwoven carbon frames having cylindrical symmetry, which are interconnected by much smaller carbon threads.[22,23] This interconnected frame system may readily collapse under harsh chemical environments and upon structural changes in the carbon walls induced by high fluorine contents. Hence, more robust turbostratic carbon frameworks are desired to withstand fluorination conditions and sustain the mesoporous structure at F/C ratios of 0.8 and higher.

A major breakthrough in the preparation of porous carbons was achieved by the direct self-assembly of phenolic resins with diblock copolymers[25] and especially triblock copolymers of general formula poly(ethylene oxide)−poly(propylene oxide)−poly(ethylene oxide), PEO−PPO−PEO.[26−30] The latter method, known as soft-templating, further reduced the number of steps and time required for the preparation of carbons compared to the hard-templating synthesis.[25] In addition, soft-templated carbons exhibit considerably larger mesopores, thicker pore walls, and higher surface areas than most carbons obtained from OMS hard templates.[31] More importantly, the cylindrical mesopores of soft-templated carbons are internal to monolithic carbon particles and are independent of small interconnecting threads supporting carbon frames as in the CMK-1 structure. The latter in combination with the thicker pore walls of soft-templated carbons result in improved mechanical, thermal, and chemical stabilities compared to those of CMK-1.

To date, the single report on fluorine-containing soft-templated carbons was for materials prepared in a one-pot synthesis route using *p*-fluorophenol/phenol−formaldehyde as carbon precursors.[32] In this report, fluorinated OMCs with covalent C−F bonds, mesopores as large as 4 nm, and surface areas approaching 1000 $m^2 g^{-1}$ were obtained.[32] However, F/C ratios were not provided, and these were probably limited by the maximum amounts of *p*-fluorophenol in the synthesis gel that allowed for the formation of a mesoporous framework. Thus, recipes to prepare soft-templated mesoporous carbon fluorides with much higher fluorine contents will be of great importance for the continuous development of high-power Li/CF_x battery technology.

In this work we demonstrate (1) that the soft-templated mesoporous carbons are ideal platforms for preparation of fluorinated carbon materials at temperatures lower than those used for graphitic carbons and (2) that such fluorinated carbon materials entail high discharging voltages and rate capabilities as cathodes for Li/CF_x batteries. The mesoporous carbons were prepared as previously reported for the self-assembly synthesis of phloroglucinol−formaldehyde in the presence of triblock EO−PO−EO copolymer BASF Pluronic F127 (labeled here as MC-R, where MC stands for mesoporous carbon and R for reference).[30,33] Furthermore, these were successfully fluorinated at various temperatures using elemental fluorine to form various MC-CF_x compounds, where x = F/C mole ratio. Also mesoporous carbons activated using a recently established procedure[33] (MA-R, where MA is mesoporous activated carbon and R is reference) were fluorinated to F/C ≈ 0.8, and the final materials (MA-CF_x) exhibited much larger mesopores and surface areas than previously reported carbon fluorides.

EXPERIMENTAL SECTION

Synthesis of Mesoporous Carbon. The MC was prepared according to a previously reported recipe.[30,34] Briefly, phloroglucinol (26 g, 206.17 mmol) and BASF Pluronic F127, $EO_{106}−PO_{70}−EO_{106}$, purchased from Sigma-Aldrich (52.0 g, 4.16 mmol) were dissolved in 200 proof ethanol (1200 mL) and 37% hydrochloric acid (10 mL) and brought to reflux. Once they were refluxing, formaldehyde (26 g, 865.8 mmol) was added, and the solution continued to be refluxed. The solid carbon polymer was filtered and carbonized under a flowing nitrogen atmosphere in a horizontal quartz tube furnace at 850 °C. The reference mesoporous carbon was labeled MC-R.

Synthesis of Nonporous Carbon. The nonporous carbon (NP) was prepared by dissolving resorcinol (2.2 g) and poly(ethylene glycol), $H(OCH_2CH_2)_nOH$, PEG (2.2 g, MW = 8000, Aldrich) in 200 proof ethanol (9 mL) and 3 M aqueous HCl (9 mL). To this solution was added 2.6 g of formaldehyde (37%), and the system was stirred for 30 min after phase separation. The polymer-rich gel was finally centrifuged at 8500 rpm for 5 min, casted on a Petri dish, and air-dried overnight and at 80 °C for 24 h. The polymer nanocomposite was carbonized using the same conditions used for the mesoporous carbon.

Activation of the Mesoporous Carbon. KOH activation was performed by heating approximately 2 g of a physical mixture of solid KOH and mesoporous carbon particles (the mass ratio of KOH to carbon was 8) in nickel crucibles and a horizontal quartz tube furnace under flowing N_2, with a heating rate of 20 °C min^{-1}, to 800 °C for 1 h. After the mixture was cooled to room temperature under N_2, the solid was washed with deionized water. *Caution: small amounts of metallic potassium that may be deposited on the inner tube surface are a potential hazard due to high reactivity with water!* The sample was then stirred in 500 mL of 0.2 M HCl solution for 30 min at 80 °C. The activated carbon was finally separated by filtration, washed with deionized water, and dried at 100 °C overnight. The activated mesoporous carbon reference sample obtained was labeled MA-R.

Fluorination Setup of Mesoporous and Nonporous Carbons. All fluorinations were conducted in a fluidized bed fluorination reactor (FBR) consisting of an 8 in. long × 1/2 in. stainless steel tube with machined ends fitted with Swagelok reducing unions in which 1/2 in. × 1/16 in. thick stainless steel fritted disks were press-fit into the 1/2 in. side of the reducing unions. The gas inlet bottom end of the reactor was connected to a 1/4 in. "J"-shaped tube that completed a "U" configuration which allowed for immersion of the assembly into a cylindrical heating or cooling bath as needed. The outlet side of the reactor tube was connected to a 3/8 in. tube which was configured to place a U trap in the 3/8 in. line to trap any generated volatile byproducts. The reactor exhaust was connected to an alumina trap with nitrogen purge to absorb unreacted fluorine and vent only oxygen and other harmless vapors. The inlet tube was connected to a mixing device consisting of a Hastings flow transducer calibrated for fluorine and a rotameter gauge flow meter for helium gas. The apparatus allowed for He/F_2 mixtures from 0% to 100% fluorine to flow into the FBR tube. All carbon samples were dried at 150 °C under vacuum overnight before fluorination. Fluorination reactions were carried out using elemental fluorine (F_2) at room temperature and higher, 150−235 °C. The samples were stored in PFA screw-cap vials under nitrogen. Fluorinated mesoporous carbon and activated mesoporous carbon materials were labeled as MC-CF_x and MA-CF_x, respectively. The nonporous carbon fluorinated sample was labeled as NP-CF_x, where x indicates the F/C ratios from EDS analysis for all samples. The detailed procedure for the fluorination of the various samples is given in the Supporting Information. Materials were compared to a commercial fluorinated carbon sample (Sigma-Aldrich) here labeled MC-$CF_{0.50}$-R.

Characterization. Energy dispersive X-ray spectroscopy (EDS) measurements were performed using a Genesis 2000 spectrometer (EDAX, Ametek) coupled to a JEOL-6060 scanning electron microscope with an accelerating voltage of 10−15 kV and an 8 mm working

Table 1. Calculated Parameters from Nitrogen Adsorption at −196 °C, Gravimetric Analysis, EDS, XPS, and Electrochemical Performance Tests for Investigated Mesoporous Carbons and Fluorinated Carbon Materials

sample	T_F[a] (°C)	V_{SP}[b] ($cm^3\ g^{-1}$)	S_{BET}[c] ($m^2\ g^{-1}$)	V_t[d] ($cm^3\ g^{-1}$)	S_{ext}[e] ($m^2\ g^{-1}$)	V_{mi}[f] ($cm^3\ g^{-1}$)	S_{mi}[g] ($m^2\ g^{-1}$)	W[h] (nm)	MF[Gi]	MF[XPSj]	MDP[k] (V vs Li/Li^+)	SC[l] (mAh g^{-1})	ED[m] (W h kg^{-1})
MC-R		0.38	272	0.38	0.28	0.03	209	9.1					
MC-$CF_{0.18}$	∼20	0.26	162	0.26	0.30	0.01	145	8.2	$C_4F_{1.052}$ ($CF_{0.26}$)	$CF_{0.20}$	2.35	283	665
MC-$CF_{0.35}$	150	0.20	137	0.20	0.17	0.01	115	8.2	$C_4F_{2.97}$ ($CF_{0.74}$)	$CF_{0.48}$	2.5	273	682
MC-$CF_{0.75}$	230	0.16	169	0.15	2.88	0.03	92	5.7	$C_4F_{2.10}$ ($CF_{0.53}$)	$CF_{0.77}$	2.2	759	1670
MC-$CF_{0.50}$	235	0.17	225	0.16	4.76	0.06	88		CF_x	$CF_{1.45}$	2.5	707	1767
NP-$CF_{0.22}$	150	0.06*	46	0.06	20.05	0.004	36	1.6	$C_4F_{1.68}$ ($CF_{0.42}$)	$CF_{0.51}$	2.1	318	668
MA-R		2.20	2157	2.18	5.64	0.51†	1032	11.0					
MA-$CF_{0.54}$	150	1.00	852	0.99	1.11	0.17†	460	11.0	$C_4F_{3.22}$ ($CF_{0.81}$)	$CF_{0.50}$	3.1	550	1705
MA-$CF_{0.55}$	200	0.98	843	0.93	15.1	0.15	488	10.5	$C_4F_{2.85}$ ($CF_{0.71}$)	$CF_{0.51}$	3.15	615	1937
$CF_{0.50}$-R		0.06*	107	0.06	4.12	0.04†	24	1.6			2.45	613	1502

[a] Fluorination temperature. [b] Single-point pore volume from adsorption isotherms at $p/p_0 \approx 0.98$ (an asterisk indicates $p/p_0 \approx 0.92$). [c] Specific surface area calculated using the BET equation in the relative pressure range of 0.05−0.20. [d] Total pore volume calculated in the α_S plot range of 2.50−7.50. [e] External surface area calculated in the α_S plot range of 2.50−7.50. [f] Micropore volume calculated in the α_S plot range of 0.75−1.00 (a dagger indicates 0.82−1.10) (*J. Colloid Interface Sci.* **1997**, *192*, 250−256). [g] Micropore surface area calculated in the α_S plot range of 0.75−1.00 (*J. Colloid Interface Sci.* **1997**, *192*, 250−256). [h] Pore width calculated according to the improved KJS method (*Langmuir* **2006**, *22*, 6757−6760) using the statistical film thickness for a nonporous reference carbon material (*Microporous Mesoporous Mater.* **2008**, *112*, 573−579). [i] Chemical composition from gravimetric analysis based on weight gain during fluorination (composition normalized by the F/C ratios in parentheses). [j] Chemical composition from XPS analysis. [k] Medium discharge potential versus Li/Li^+. [l] Specific capacity under a discharge current of C/20. [m] Energy density calculated from the product of the medium discharge potential and specific capacity.

distance. X-ray photoelectron spectroscopy (XPS) data were collected using a PHI 3056 spectrometer with an Al anode source operated at 15 kV and an applied power of 350 W. Samples were manually pressed between two pieces of indium foil; the piece of In foil with the sample on it was then mounted to the sample holder with a piece of carbon tape (Nisshin EM Co. Ltd.). Adventitious carbon was used to calibrate the binding energy shifts of the sample (C1s, 284.8 eV). High-resolution data were collected at a pass energy of 5.85 eV with a 0.05 eV step size and a minimum of 100 scans to improve the signal-to-noise ratio; lower resolution survey scans were collected at a pass energy of 93.5 eV with a 0.5 eV step size and a minimum of 25 scans. Peak assignments were made according to previously reported graphite intercalation compounds (GICs).[35] Nitrogen adsorption isotherms were measured at −196 °C using a TriStar 3000 volumetric adsorption analyzer manufactured by Micromeritics Instrument Corp. (Norcross, GA). Before adsorption measurements the carbon powders were degassed in flowing nitrogen for 1−2 h at 200 °C. The specific surface area of the samples was calculated using the Brunauer−Emmett−Teller (BET) method within the relative pressure range of 0.05−0.20.[36] Pore size distributions were calculated using the Barrett−Joyner−Halenda (BJH) algorithm for cylindrical pores according to the Kruk−Jaroniec−Sayari (KJS) method calibrated for pores of up to 10 nm[37] and statistical film thickness for a reference carbon adsorbent[38] also used for the α_S plot analysis.[39] Coin cells (CR2032) were assembled to test the electrochemical performance of the various carbon fluoride materials. The cathode was prepared by spreading a slurry of active material (75 wt %), carbon black (10 wt %), and poly(vinylidene fluoride) (PVDF; 15 wt %) in *N*-methyl-2-pyrrolidone (NMP) onto Al foil. The active material loading was 1−2 mg cm^2. The electrodes were dried in a vacuum oven at 120 °C overnight before being transferred into an argon-filled glovebox (VAC OMNI-LAB). The anode was a lithium metal disk, and the separator was Cegard 2034. The C rate calculation was based on the theoretical capacity. The electrolyte was 1.0 M $LiBF_4$ in ethylene carbonate/dimethyl carbonate/diethylene carbonate (EC/DMC/DEC; 1:1:1, vol %). The coin cells were discharged on an Arbin BT2000 instrument at room temperature by applying a constant current with a cutoff voltage of 1.5 V. A discharge rate ranging from 0.05C to 5C was used.

RESULTS AND DISCUSSION

The F/C ratios for all fluorinated samples were largely dependent on the fluorination temperature used for both pristine and activated carbons as shown in Table 1. For instance, by increasing the temperature for fluorination of MC-R from room temperature to 230 °C, the F/C ratio increased from 0.18 to 0.75, respectively. Furthermore, after a stepwise fluorination route of the same sample at 235 °C, the F/C decreased to 0.50. For the latter, the determination of its F/C ratio based on gravimetric analysis was not possible since mass was lost during fluorination. Such mass loss may have occurred as a result of the formation of volatile perfluoroalkanes and of oxygen-containing products at the high temperature used to prepare this material (235 °C). Also interesting was the sample MC-$CF_{0.75}$, for which the gravimetric analysis indicated a F/C ratio of ∼0.5. None of these ratios corresponded to the white-gray color observed for this compound, typical of materials with F/C higher than 0.9,[2] thus indicating that this sample was heterogeneously fluorinated.

XPS analysis, see Table S1 with peak assignments[40] and Figure S1 in the Supporting Information, and representative spectra in Figure 1 show the same semi-ionic CF_2 moieties present in all investigated samples (binding energy 688.0 eV).[40−42] Additional F species were identified for the nonporous carbon sample (NP-CF_x) investigated for comparison, namely, NP-$CF_{0.22}$, at 689.5 eV (Figure 1a), and mesoporous MC-$CF_{0.35}$, at 685.9 eV, corresponding to covalent and ionic F species, respectively. In addition to that, most samples have small concentrations of surface oxide species (approximately 1 wt %), usually found on mesoporous carbon samples. These binding energies are fairly consistent with C−O species (∼534 eV) with the exception of MC-$CF_{0.35}$, for which a sizable concentration of C═O species was identified (∼532 eV).[43] Analysis of the C1s XPS data revealed the formation of a rich array of carbon-based species with various compositions and structures (cf. Supporting Information). The F-containing moieties are all sp^3-type species

dx.doi.org/10.1021/cm2012395 |*Chem. Mater.* 2011, 23, 4420–4427

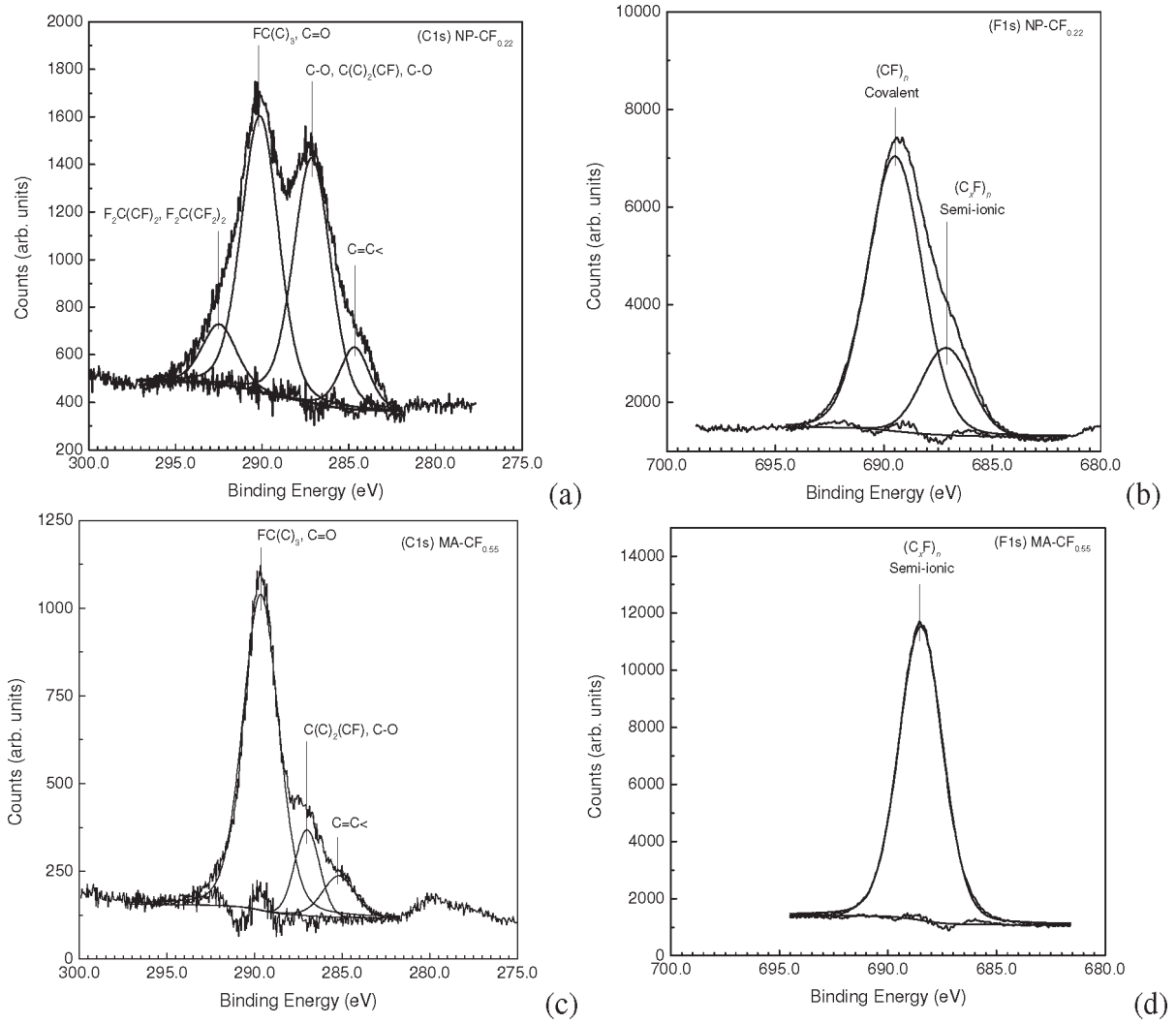

Figure 1. XPS spectra, peak fittings, and assignments for C1s (a) and F1s (b) for NP-$CF_{0.22}$ and C1s (c) and F1s (d) for MA-$CF_{0.55}$.

[C−$\underline{C}(CF)_3$ (~288 eV)$F\underline{C}(C)_3$ (~289 eV), $F\underline{C}(CF)_3$ (~291 eV), $F_2\underline{C}(CF)_2$ (~292.5 eV)] due to the breaking of sp^2 bonds in the graphitic starting material during the addition of F. The carbon-rich sample MC-$CF_{0.18}$ has the largest concentrations of sp^2-type C═C (284.8 eV) species, consistent with its stoichiometry. In contrast, the MC-$CF_{0.75}$ sample has no evident sp^2 graphitic species, which is consistent for materials with such large F contents. All other samples exhibited intermediate concentrations of sp^2 graphitic type carbon and sp^3 C−F based species with concentrations between those found for MC-$CF_{0.18}$ (~52 wt % sp^2) and MC-$CF_{0.50}$ (~4 wt % sp^2). Further investigation of the XPS data provides evidence for the distributions and the bonding of F in these carbons. The MC-$CF_{0.75}$ sample, with the highest F/C ratios based on EDS, has very high concentrations of $FC(CF)_3$ and $C(CF)_3$ and consequently a low concentration of isolated graphene carbons without fluorinated neighbor species. Samples such as MC-$CF_{0.18}$ and NP-$CF_{0.22}$ (Figure 1b) samples have high concentrations of $F_2C(CF)_2$ (292.0 eV) and $FC(CF)_3$ (290.2 eV) moieties, which would be electrically isolated, but large concentrations of $\underline{C}(C)_2(CF)$ species (286 eV), which indicates the F species are concentrated on the more exposed carbon surfaces, and not homogeneously distributed, presumably due to the low temperature of reaction and some fluorine selectivity. In contrast, the samples MC-$CF_{0.35}$, MA-$CF_{0.54}$, MA-$CF_{0.55}$ (Figure 1c,d), MC-$CF_{0.75}$, and MC-$CF_{0.50}$ have high concentrations of $FC(C)_3$ moieties shown by a peak centered at 289.3 eV and a second peak with the $C(CF)(C)_2$ characteristic centered at 286.0 eV. These peaks may indicate a more optimized distribution of F in the carbon matrix and more C−C bonding, which is required for electrical conductivity, since these are seen in addition to $FC(CF)_3$ (291 eV) and $F_2\underline{C}(CF)_2$ (292.5 eV) groups, which would be less electrochemically active. Higher concentrations of F result in more $FC(CF)_3$ moieties (291 eV), and those of unfluorinated sp^3 C having fluorinated or oxygen-substituted neighbor species (286.0−287.0 eV) indicate that the C−C bonds are not as homogenously dispersed, i.e., $C(CF)_3$. Elemental analysis data showed F/C ratios similar to those found by EDS analysis. Because of the many different parameters used for each fluorination reaction, a direct correlation between the extent of fluorination and the temperatures used is difficult. However, the most homogeneously fluorinated materials were those obtained after reactions at 150 °C, namely, MC-$CF_{0.35}$, as well as those fluorinated after chemical activation, MA-$CF_{0.54}$ and MA-$CF_{0.55}$. The chemical activation of mesoporous carbons by KOH may have introduced a large number of sp^3 carbons linked to C−C in the carbon walls. The former sites facilitated

dx.doi.org/10.1021/cm2012395 |*Chem. Mater.* 2011, 23, 4420–4427

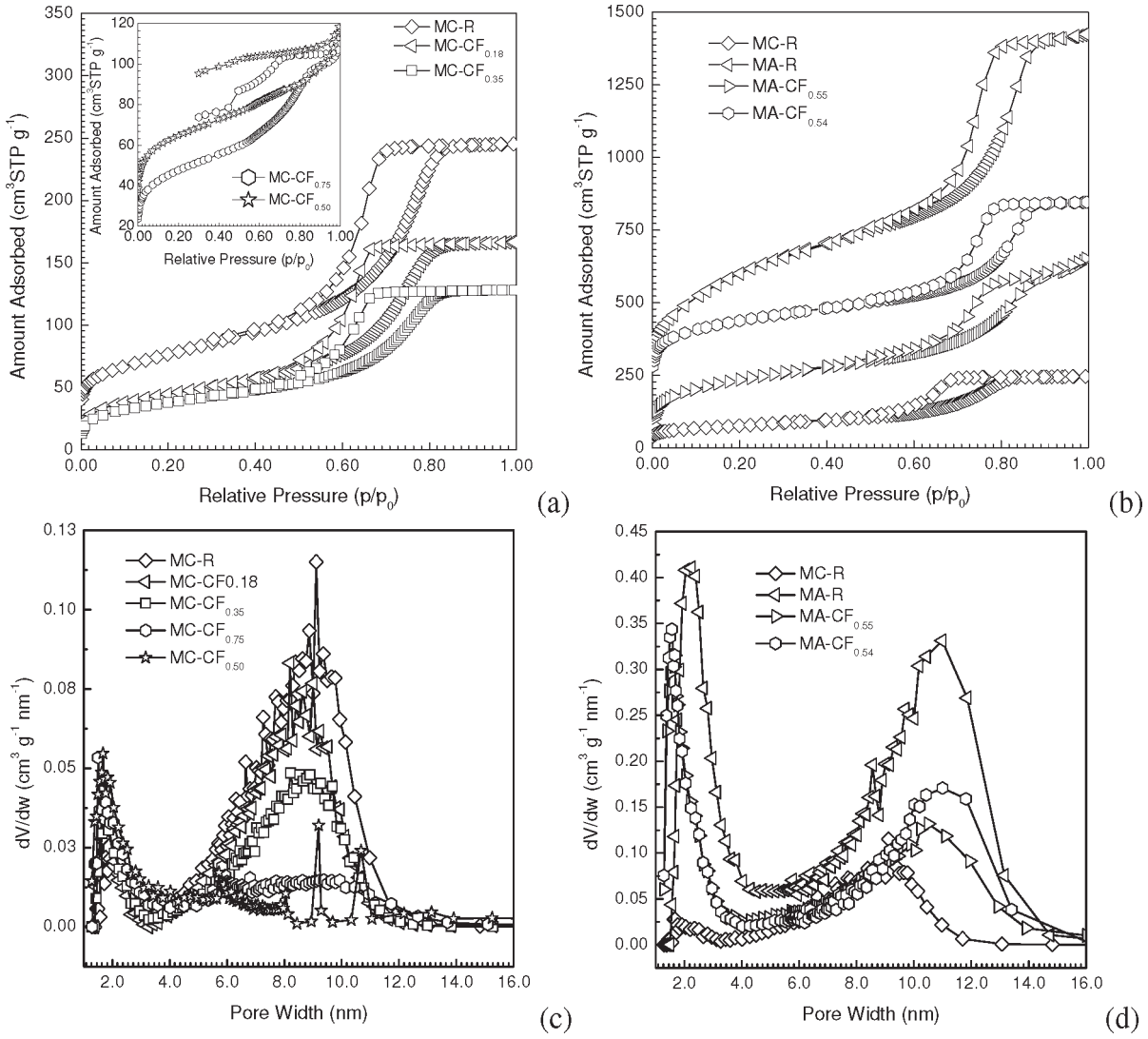

Figure 2. Nitrogen adsorption isotherms at −196 °C for fluorinated mesoporous carbons before (a) and after (b) activation and respective calculated pore size distributions (c, d). The adsorption isotherm of MA-$CF_{0.54}$ in (b) was vertically offset by 200 cm^3 STP g^{-1}.

the surface fluorination of these carbons, helping to preserve the C−C backbone structure. Finally, for nonactivated samples fluorinated at low reaction temperatures, or with very small starting exposed surfaces, fluorination proceeded with disruption of the C−C backbone and formation of F−C−F species.

Nitrogen adsorption isotherms for the pristine, activated mesoporous carbons and their respective fluorinated products are shown in Figure 2a,b. In general, all fluorinations lead to a consequent reduction by more than 50% in the pore volumes and specific surface areas of fluorinated compounds compared to the starting carbons (see calculated results in Table 1). These adsorption isotherms are type IV with steep capillary condensation steps and H1 hysteresis loops typical of materials with large and uniform mesopores.[36] The H1 hysteresis loops further indicate the absence of pore constrictions in most materials. The adsorption branches of the isotherms for MC-$CF_{0.50}$ and MC-$CF_{0.75}$ samples exhibit multiple and poorly defined condensation steps, revealing broad distributions of mesopores. In addition, the hysteresis loops for MC-$CF_{0.50}$ and MC-$CF_{0.75}$ indicate large amounts of constricted pores.[36] The adsorption isotherm for the NP-$CF_{0.22}$ sample (see Figure S2a in the Supporting Information) is type 2, characteristic of nonporous materials, whereas for the commercial sample $CF_{0.50}$-R despite, its low pore volume, the isotherm resembles type 1 for microporous materials (Figure S2a).[36] The sample $CF_{0.50}$-R also shows slightly higher gas uptake at lower relative pressures than NP-$CF_{0.22}$ due to small amounts of micropores present in the former; see Table 1 and the calculated pore size distributions[37,38] in Figure S2b. In addition, the H3-type hysteresis loop[36] for $CF_{0.50}$-R further reveals the existence of some textural mesopores, which are formed by particle aggregates. The hysteresis loop for the activated carbon material shifted to higher relative pressures than that of the starting MC-R sample as a result of the enlargement of mesopores[36] during activation. The latter was confirmed by the calculated pore size distributions,[37,38] Figure 2cd, confirming the pore enlargement by approximately 2 nm. The mesopore and micropore volumes from the α_S plot analysis[36,44] for the activated sample increased by 1.32 and 0.48 cm^3 g^{-1},[36,44] respectively (Table 1). The specific surface areas increased from ∼300 m^2 g^{-1} for MC-R to 2157 m^2 g^{-1}

dx.doi.org/10.1021/cm2012395 |Chem. Mater. 2011, 23, 4420–4427

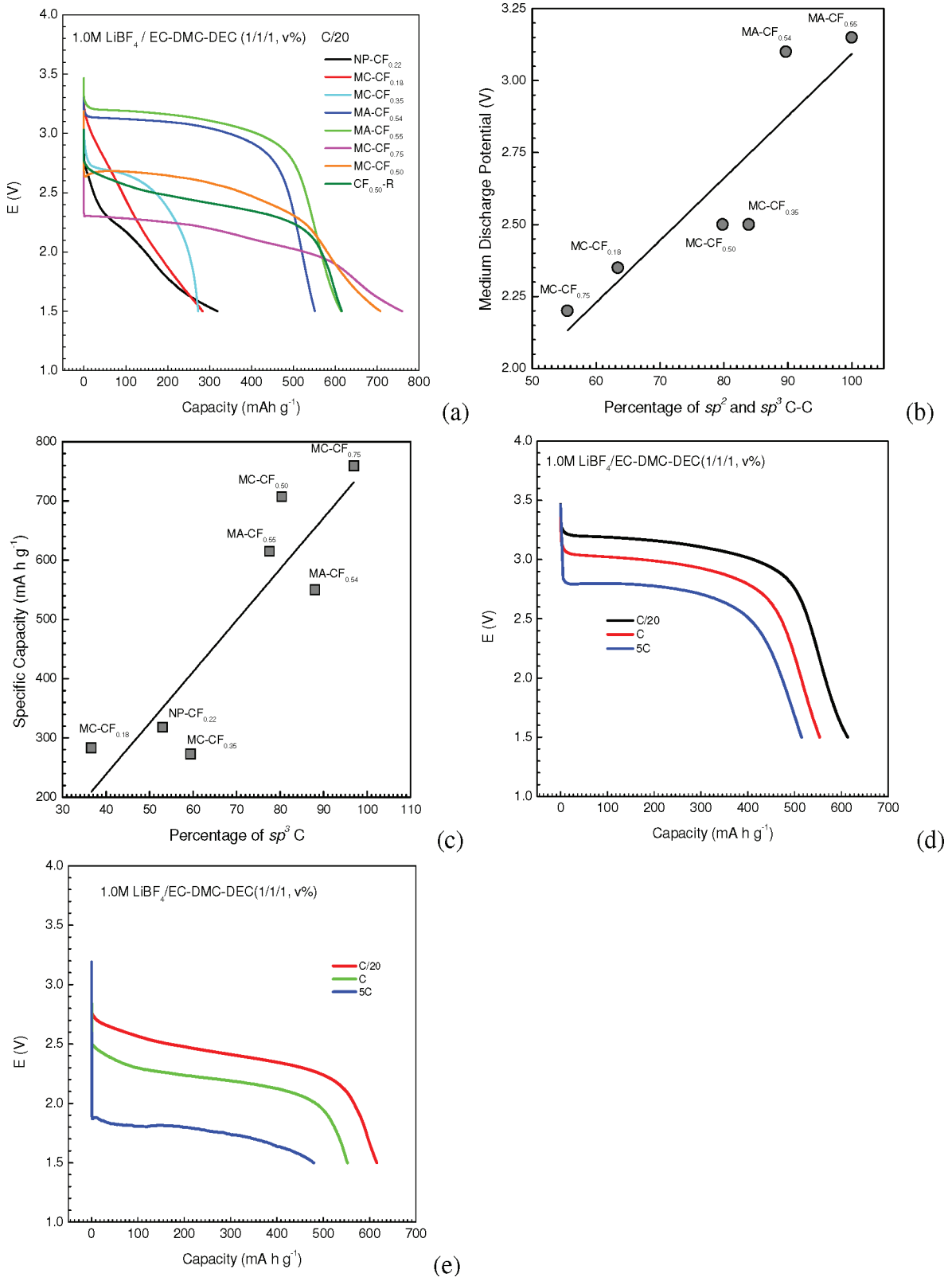

Figure 3. Discharge profile of Li/CF_x cells at a rate of C/20 and in comparison to a commercial sample, $CF_{0.50}$-R (a). Medium discharge potential as a function of the percentage of sp^2 and sp^3 carbon−carbon bonds from XPS analysis [C−C (~284.8 eV), $\underline{C}(C)_2(CF)$ (~286 eV), C−$\underline{C}(CF)_3$ (~288 eV), F$\underline{C}(C)_3$ (~289 eV)] (b). Specific capacity as a function of the percentage of sp^3 carbon from XPS analysis [C−$\underline{C}(CF)_3$ (~288 eV), F$\underline{C}(C)_3$ (~289 eV), F$\underline{C}(CF)_3$ (~291 eV), $F_2\underline{C}(CF)_2$ (~292.5 eV)] (c). Discharge profiles of Li/CF_x cells based on samples MA-$CF_{0.55}$ (d) and $CF_{0.50}$-R (e) at different discharge rates.

dx.doi.org/10.1021/cm2012395 |*Chem. Mater.* 2011, 23, 4420–4427

after activation. However, after fluorination of the MA-R sample, the specific surface areas for MA-$CF_{0.54}$ and MA-$CF_{0.55}$ went from 2157 $m^2\ g^{-1}$ to as low as 843 $m^2\ g^{-1}$. Furthermore, while the mesopore widths of fluorinated activated carbons were similar to those of the starting activated carbons, those for fluorinated mesoporous carbons prepared directly from MC-R were nearly 1 nm narrower than those of the starting carbon sample. In addition, fluorinated carbons obtained from activated materials still exhibited larger surface areas, pore volumes, and mesopores than the pristine MC-R and the nonactivated fluorinated materials (Table 1). As also seen by these results, the final adsorption properties changed with the temperature and consequently with the final fluorine contents, providing additional evidence for the large extent of fluorination and homogeneity of the fluorine distribution in these materials.

Depending on the extent of fluorination, the hybridization of carbon atoms changes from sp^2 to sp^3,[17,45] whereas extensive fluorination will result in the formation of intercalation fluorine compounds with C−F bonds of semi-ionic and ionic character.[2,7] The highest discharge voltages vs Li are expected for materials having the most ionic C−F bonds.[46] This is observed for the MC and NP materials where the MC-$CF_{0.35}$ sample exhibited a high (for the MC samples) 2.5 V discharge voltage as a result of the ionic character of the C−F bonds observed in the XPS whereas the nonporous NP-$CF_{0.22}$ has the most covalent C−F bond and also the lowest discharge potential compared to all other samples, 2.10 V. However, ionic-covalent arguments cannot be used to explain the large variations in voltages for the other samples which have semi-ionic C−F. Figure 3a shows the discharge capacities of the various nonactivated and activated fluorinated mesoporous carbons at a current density of C/20 (40 mA g^{-1}, 44.5 mA cm^{-1}). For comparison, commercial $CF_{0.50}$-R (Aldrich) was cycled under the same current rate. The discharge profiles of these carbon fluorides greatly differ on the basis of the carbon precursors and on the basis of their F/C ratios. For instance, while for the less fluorinated carbon fluoride MC-$CF_{0.18}$ the discharge starts at 3.2 V and continually drops to 1.5 V with two barely visible voltages, for the nonporous material (NP-$CF_{0.22}$) these two stages are more pronounced. For the latter the voltage quickly drops to 2.8 V from an open cell voltage of 3.3 V at the onset of the discharge. With increasing F/C ratios, as in MC-$CF_{0.35}$, the discharge plateau becomes even more pronounced and levels off until the capacity reaches 150 mA h g^{-1}, after which the voltage quickly drops to 1.5 V. With the highest fluorine content achieved in this series, the material MC-$CF_{0.75}$ exhibits the highest discharge capacity among all nonactivated samples; however, the discharge plateau of 2.2 V is the lowest, which is mainly due to the strong covalent character of the C−F bond in this material as evident in the XPS data.[4,46] The most striking differences are between $CF_{0.50}$-R and MA-$CF_{0.55}$, both containing similar fluorine contents according to EDS analysis. Under a current rate of C/20, the batteries based on $CF_{0.50}$-R and MA-$CF_{0.55}$ deliver a similar specific capacity of 613−615 mA h g^{-1} (Table 1). However, MA-$CF_{0.55}$ shows a net increase of 0.70 V in the medium discharge potential compared to $CF_{0.50}$-R (2.45 V). As a general trend, the medium discharge potentials of the cells increased with increasing total C−C interactions (both sp^3 and sp^2 carbon−carbon bonding, i.e., C−C (∼284.8 eV), $\underline{C}(C)_2(CF)$ (∼286 eV), C−$\underline{C}(CF)_3$ (∼288 eV), and F$\underline{C}(C)_3$ (∼289 eV)) from the XPS analysis (Table S1, Supporting Information) shown by correlation in Figure 3b. This trend is logical since C−C bonds in these carbonaceous frameworks are directly responsible for the electron transport in the particles; the sp^3 C atoms are bound to both F and sp^2 C atoms in conjugated π-systems. The nonporous NP-$CF_{0.22}$ sample is excluded from this trend because of the lack of porosity, which kinetically limits the cell and the high concentration of covalent C−F bonds (689.5 eV) The specific capacity scales as a function of sp^3-type carbon in the samples, i.e., the sum of the C−$\underline{C}(CF)_3$ (∼288 eV), F$\underline{C}(C)_3$ (∼289 eV), F$\underline{C}(CF)_3$ (∼291 eV), and $F_2\underline{C}(CF)_2$ (∼292.5 eV) species; see Figure 3c. This parameter increased with increasing sp^3 C atoms, which are linked to surface $-CF_2/-CF_3$ moieties responsible for the large Li storage.[2,9,18,19]

Clearly, to optimize the electrochemical properties of the cell requires high concentrations of sp^3 F sites (for Li storage) and C−C bonding for electrical conduction and high surface areas to maximize the number of F sites (related to capacity). The MA-$CF_{0.55}$ sample fulfills these requirements, having 78% $FC(C)_3$ moieties in the sample and few electrically isolated $FC(CF)_3$ species. As shown in Figure 3d the batteries based on MA-$CF_{0.55}$ not only show higher discharge potentials but also show good rate capabilities due to the accessible micro- and mesopores of the fluorinated carbon electrode. Under a C rate (623 mA g^{-1}, 775 mA cm^{-2}) the latter delivers a specific capacity of 554 mA h g^{-1} with a medium discharge potential of 3.0 V; by increasing the discharge rate to 5C (3136 mA g^{-1}, 3994 mA cm^{-2}), the specific capacity slightly decreases to 515 mA h g^{-1}, while exhibiting an impressive medium discharge potential of 2.75 V. In contrast, the specific capacities and medium discharge potentials of the cell based on $CF_{0.50}$-R decrease from 503 mA h g^{-1} and 2.2 V at a C rate to as low as 480 mA h g^{-1} and 1.8 V at a 5C rate, respectively (Figure 3e). This is due to the lower surface area and more electrically isolated $FC(CF)_3$ species (20%), which limit reaction kinetics.

Higher discharge potentials are desirable for practical applications, since a cell based on the same amount of active electrode material and under the same discharge conditions will deliver not only high power, but also more energy. For example, compared with the battery based on $CF_{0.50}$R, the increases in power and energy densities for the battery based on MA-$CF_{0.55}$ are 28.6% and 29.0% at a C/20 discharge rate and increased to 36.4% and 50.2% at a 1C discharge rate and 52.8% and 63.9% at a 5C discharge rate, respectively. The high rate capabilities of these mesoporous carbon fluorides show the major improvements over previously reported nonporous carbon nanofibers with similar fluorine contents that offered similar capacities only at much lower potentials.[9] The rate capabilities of the mesoporous carbon fluorides also make these better for electrode applications than graphite fluorides with higher fluorine contents. The latter offered similar discharge potential and capacity, but under much lower discharge current density.[4,21]

CONCLUSIONS

In summary, our results demonstrate that mesoporous carbons and activated mesoporous carbon materials can be fluorinated using elemental fluorine at temperatures much lower than those used for graphitic carbons because of their hierarchical pore structure of micro- and mesopores. Also, the extent and homogeneity of fluorination can be controlled by the selected temperature and time on stream. In this way, mesoporous carbon fluorides with narrow distributions of mesopores from 6 to 11 nm in width and specific surface areas as large as 852 $m^2\ g^{-1}$ can be prepared in large yields. Even more, these materials offer several

advantages over commercial carbon fluorides with similar fluorine contents when tested as cathodes in Li/CF_x batteries, such as higher discharge potential, faster reaction kinetics under high current densities, and higher energy and power densities. These novel carbon fluorides are ideal candidates for practical applications in energy storage and conversion devices where high power and energy densities are primary requirements.

■ ASSOCIATED CONTENT

Supporting Information. Detailed fluorination reactions at various temperatures, Figure S1 with additional selected XPS spectra and peak assignments, Figure S2 showing nitrogen adsorption at −196 °C and calculated pore size distributions for a nonporous fluorinated carbon and a commercial carbon fluoride sample, and Table S1 with complete XPS peak assignments and weight percentages of carbon, fluorine, and oxygen. This material is available free of charge via the Internet at http://pubs.acs.org.

■ AUTHOR INFORMATION

Corresponding Author

*Fax: (865) 576-5235. Phone: (865) 576-7307. E-mail: dais@ornl.gov (S.D.); sunx@ornl.gov (X.-G.S.); veithgm@ornl.gov (G.M.V.).

■ ACKNOWLEDGMENT

The main part of this work was supported by the U.S. Department of Energy's Office of Basic Energy Science, Division of Materials Sciences and Engineering, under contract with UT-Battelle, LLC. P.F.F. and S.M.M. were supported as part of the Fluid Interface Reactions, Structures and Transport (FIRST) Center, an Energy Frontier Research Center funded by the U.S. Department of Energy, Office of Science, Office of Basic Energy Sciences, under Award Number ERKCC61.

■ REFERENCES

(1) Nakajima, T. *J. Fluorine Chem.* **1999**, *100*, 57.
(2) Nakajima, T.; Touhara, H.; Okino, F. *Actual. Chim.* **2006**, 119.
(3) Linden, D. *Handbook of Batteries*; McGraw-Hill: New York, 1994; Vol. 2.
(4) Lam, P.; Yazami, R. *J. Power Sources* **2006**, *153*, 354.
(5) Nakajima, T. *Macromol. Symp.* **1994**, *82*, 19.
(6) Nakajima, T.; Ando, H.; Kawaguchi, M.; Watanabe, N. *Denki Kagaku* **1985**, *53*, 181.
(7) Palchan, I.; Crespin, M.; Estradeszwarckopf, H.; Rousseau, B. *Chem. Phys. Lett.* **1989**, *157*, 321.
(8) Chamssedine, F.; Dubois, M.; Guerin, K.; Giraudet, J.; Masin, F.; Ivanov, D. A.; Vidal, L.; Yazami, R.; Hamwi, A. *Chem. Mater.* **2007**, *19*, 161.
(9) Yazami, R.; hamwi, A.; Guerin, K.; Ozawa, Y.; Dubois, M.; Giraudet, J.; Masin, F. *Electrochem. Commun.* **2007**, *9*, 1850.
(10) Nakajima, T.; Kasamatsu, S.; Matsuo, Y. *Eur. J. Solid State Inorg. Chem.* **1996**, *33*, 831.
(11) Hamwi, A.; Alvergnat, H.; Bonnamy, S.; Beguin, F. *Carbon* **1997**, *35*, 723.
(12) Matsuo, Y.; Nakajima, T. *Electrochim. Acta* **1996**, *41*, 15.
(13) Matsuo, Y.; Nakajima, T.; Kasamatsu, S. *J. Fluorine Chem.* **1996**, *78*, 7.
(14) Claves, D.; Giraudet, J.; Hamwi, A.; Benoit, R. *J. Phys. Chem. B* **2001**, *105*, 1739.
(15) Hamwi, A. *J. Phys. Chem. Solids* **1996**, *57*, 677.
(16) Jia, J. F.; Wu, H. S.; Xu, X. H.; Zhang, X. M.; Jiao, H. J. *J. Am. Chem. Soc.* **2008**, *130*, 3985.
(17) Hagaman, E. W.; Murray, D. K.; Del Cul, G. D. *Energy Fuels* **1998**, *12*, 399.
(18) Naga, K.; Nakajima, T.; Aimura, S.; Ohzawa, Y.; Zemva, B.; Mazej, Z.; Groult, H.; Yoshida, A. *J. Power Sources* **2007**, *167*, 192.
(19) Nakajima, T.; Shibata, S.; Naga, K.; Ohzawa, Y.; Tressaud, A.; Durand, E.; Groult, H.; Warmont, F. *J. Power Sources* **2007**, *168*, 265.
(20) Nakajima, T.; Matsuo, Y.; Zemva, B.; Jesih, A. *Carbon* **1996**, *34*, 1595.
(21) Nakajima, T.; Koh, M.; Gupta, V.; Zemva, B.; Lutar, K. *Electrochim. Acta* **2000**, *45*, 1655.
(22) Ryoo, R.; Joo, S. H.; Jun, S. *J. Phys. Chem. B* **1999**, *103*, 7743.
(23) Ryoo, R.; Joo, S. H.; Kruk, M.; Jaroniec, M. *Adv. Mater.* **2001**, *13*, 677.
(24) Li, Z. J.; Del Cul, G. D.; Yan, W. F.; Liang, C. D.; Dai, S. *J. Am. Chem. Soc.* **2004**, *126*, 12782.
(25) Liang, C. D.; Hong, K. L.; Guiochon, G. A.; Mays, J. W.; Dai, S. *Angew. Chem., Int. Ed.* **2004**, *43*, 5785.
(26) Meng, Y.; Gu, D.; Zhang, F. Q.; Shi, Y. F.; Cheng, L.; Feng, D.; Wu, Z. X.; Chen, Z. X.; Wan, Y.; Stein, A.; Zhao, D. Y. *Chem. Mater.* **2006**, *18*, 4447.
(27) Meng, Y.; Gu, D.; Zhang, F. Q.; Shi, Y. F.; Yang, H. F.; Li, Z.; Yu, C. Z.; Tu, B.; Zhao, D. Y. *Angew. Chem., Int. Ed.* **2005**, *44*, 7053.
(28) Zhang, F. Q.; Meng, Y.; Gu, D.; Yan, Y.; Yu, C. Z.; Tu, B.; Zhao, D. Y. *J. Am. Chem. Soc.* **2005**, *127*, 13508.
(29) Wang, X. Q.; Liang, C. D.; Dai, S. *Langmuir* **2008**, *24*, 7500.
(30) Liang, C. D.; Dai, S. *J. Am. Chem. Soc.* **2006**, *128*, 5316.
(31) Wan, Y.; Yang, H. F.; Zhao, D. Y. *Acc. Chem. Res.* **2006**, *39*, 423.
(32) Wan, Y.; Qian, X.; Jia, N. Q.; Wang, Z. Y.; Li, H. X.; Zhao, D. Y. *Chem. Mater.* **2008**, *20*, 1012.
(33) Yu, L. T.; Jiang, X. F.; Wang, L. X.; Li, Z. K.; Wu, D.; Zhou, X. G. *Eur. J. Org. Chem.* **2010**, 5560.
(34) Wang, X. Q.; Lee, J. S.; Tsouris, C.; DePaoli, D. W.; Dai, S. *J. Mater. Chem.* **2010**, *20*, 4602.
(35) Sato, Y.; Itoh, K.; Hagiwara, R.; Fukunaga, T.; Ito, Y. *Carbon* **2004**, *42*, 3243.
(36) Kruk, M.; Jaroniec, M. *Chem. Mater.* **2001**, *13*, 3169.
(37) Jaroniec, M.; Solovyov, L. A. *Langmuir* **2006**, *22*, 6757.
(38) Choma, J.; Gorka, J.; Jaroniec, M. *Microporous Mesoporous Mater.* **2008**, *112*, 573.
(39) Kruk, M.; Jaroniec, M.; Gadkaree, K. P. *J. Colloid Interface Sci.* **1997**, *192*, 250.
(40) Sato, Y.; Itoh, K.; Hagiwara, R.; Fukunaga, T.; Ito, Y. *Carbon* **2004**, *42*, 3243.
(41) Nansé, G.; Papirer, E.; Fioux, P.; Moguet, F.; Tressaud, A. *Carbon* **1997**, *35*, 175.
(42) Read, J. A.; Behl, W. K. *Electrochem. Solid State Lett.* **2009**, *12*, A16.
(43) Kundu, S.; Wang, Y.; Xia, W.; Muhler, M. *J. Phys. Chem. C* **2008**, *112*, 16869.
(44) Gardner, L.; Kruk, A.; Jaroniec, M. *J. Phys. Chem. B* **2001**, *105*, 12516.
(45) Guerin, K.; Pinheiro, J. P.; Dubois, M.; Fawal, Z.; Masin, F.; Yazami, R.; Hamwi, A. *Chem. Mater.* **2004**, *16*, 1786.
(46) Root, M. J.; Dumas, R.; Yazami, R.; Hamwi, A. *J. Electrochem. Soc.* **2001**, *148*, A339.